Precipitable Water Characteristics during the 2013 Colorado Flood using Ground-Based GPS Measurements

Hannah K. Huelsing[1,2], Junhong Wang[2], Carl Mears[3], and John J. Braun[1]

1. Constellation Observing System for Meteorology, Ionosphere, and Climate Program Office
   University Corporation for Atmospheric Research
   3300 Mitchell Lane, Boulder, CO 80301
2. Department of Atmospheric and Environmental Sciences
   University at Albany, SUNY
   1400 Washington Avenue, Albany, NY 12222
3. Remote Sensing Systems
   444 10th Street, #200
   Santa Rosa, CA 95401

Corresponding Author:
Hannah K. Huelsing
Constellation Observing System for Meteorology, Ionosphere, and Climate Program
University Corporation for Atmospheric Research
3300 Mitchell Lane, Boulder, CO 80301
Phone: (303) 497-2606; Email: huelsing@ucar.edu

Abstract

During 9th-16th September 2013, the Front Range region of Colorado experienced heavy rainfall that resulted in severe flooding. Precipitation totals for the event exceeded 450 mm, damages to public and private properties were estimated to be over $2 billion, and nine lives were lost. This study analyzes the characteristics of precipitable water (PW) surrounding the event using 10 years of high-resolution GPS PW data in Boulder, Colorado, which was located within the region of maximum rainfall. PW in Boulder is dominated by seasonal variability with an average summertime maximum of 36 mm. In 2013, the seasonal PW maximum extended into early September and the September monthly mean PW exceeded the 99th percentile of climatology with a value 25% higher than the 40 year climatology. Prior to the flood, around 18 UTC on 8 September, PW rapidly increased from 22 mm to 32 mm and remained around 30 mm for the entire event as a result of the nearly saturated atmosphere. The frequency distribution of September PW for Boulder is typically normal, but in 2013 the distribution was bimodal due to a combination of above average PW values from September 1st-15th and much drier conditions from 16th-30th September. The above normal, near saturation PW values during the flood were the result of large-scale moisture transport into Colorado from the eastern tropical Pacific and the Gulf of Mexico. This moisture transport was the product of a stagnating, cutoff low over the southwestern United States working in conjunction with an anticyclone located over the southeastern United States. A blocking ridge located over the Canadian Rocky Mountains kept both of the synoptic features in place over the course of several days, which helped to provide continuous moisture to the storm, thus enhancing the accumulated precipitation totals.

Keywords

Precipitable Water, GPS, 2013 Colorado Flood, Extreme Precipitation

1. Introduction

During 9th-16th September 2013, multiple local and state precipitation records were broken when low-level, easterly flow interacted with an anomalous moisture pool over the Front Range region of Colorado to produce one of the largest floods in state history (Colorado Climate Center, 2013). The heaviest and most persistent rainfall occurred on the 11th and 12th of September, with a maximum centered over Boulder and Larimer counties (Fig. 1). In the hardest hit areas, total precipitation accumulation exceeded 450 mm (17.7 in) (Gochis et al. 2015). The city of Boulder set multiple records, observing 292.6 mm over the course of two days and 341.8 mm over the course of three days. The resultant flooding claimed nine lives and caused 1,100 documented landslides. Damages to public and private properties were estimated to be over $2 billion (Gochis et al. 2015).

The following summary of the September 2013 event was first presented in Gochis et al. (2015). Surface temperatures were in the 16-18 °C (60-64 °F) range and precipitable water (PW) values were high. Periods of heavy precipitation exceeding 25 mm (1 in) per hour, along with flooding, began on the evening of 11th September, with the heaviest portions over the Front Range, the area outlined in Fig. 1. The mountainous region between Boulder and Estes Park experienced the heaviest rain rates, which ranged from 25-50 mm (1-2 in) per hour and resulted in an overnight total exceeding 200 mm (8 in). Somewhat lighter rainfall continued into the 12th, becoming intense once more during the afternoon hours and increasing rainfall totals to over 380 mm (15 in) in the Boulder to Estes Park region. By the 13th, precipitation had finally lessened to intermittent showers and widespread drizzle, finally clearing on the 14th. A final surge of moisture occurred on

92 the 15th and resulted in 25-50 mm (1-2 in) of widespread, moderate rainfall on soils that
93 were already saturated, thus increasing the amount of runoff.
94 This event was uncharacteristic, not only because of its rainfall amounts but also
95 because of the time of year in which it occurred. Petersen et al. (1999) examined the
96 climatology of precipitation events over the Front Range region and found that, while a
97 majority of events occur between April and October, the convective classification of the
98 events differs depending on what time of year the convection occurs in. There are two
99 peaks in the event distribution, the first of which occurs in late May to early June.
100 Precipitation events during this time are synoptic, or large, scale and quasi-stationary.
101 The precipitation in these events is enhanced orographically and locally, and is typically
102 widespread and of moderate intensity. The second peak in precipitation events occurs
103 from late July into early September with a pronounced maximum frequency from late
104 July into early August. The storms in these events generally have a small areal extent and
105 are highly convective. The September 2013 event was quasi-stationary and synoptic with
106 precipitation controlled by localized and orographic enhancements. The areal extent of
107 the 2013 event was large and the rainfall was of moderate intensity. According to the
108 climatology completed by Petersen et al. (1999), this type of event was more typical of
109 storms which occur in late May to early June. However, this event occurred at a time of
110 year when precipitation tends to be highly convective and of small areal extent, so the
111 timing, as well as the amount of rainfall, was abnormal.
112 In another study which examined the climatology of rainfall events in Colorado,
113 Mahoney et al. (2015) found that the region of Colorado east of the Continental Divide
114 does not generally experience heavy precipitation events in the fall because it is during

this time of year that the region experiences seasonal atmospheric drying. They did note that there was enhanced climatological variability in September and October, making it difficult to place these months into the same category as the drier months (November-February). In general, east of the Continental Divide experiences most of its precipitation in the spring and summer months, with the Front Range receiving a majority of its moisture in the spring. However, extreme precipitation events are not limited to these seasons and can also occur in fall and winter months.

Flooding due to extreme precipitation events can occur at any time of the year because all elevations in all seasons are prone to experiencing heavy precipitation. This is partially represented by the dates in Table 1, which compares the September 2013 event to previous heavy precipitation events in Northern Colorado history that resulted in catastrophic flooding (Colorado Climate Center; Maddox et al. 1977; Petersen et al. 1999; Gochis et al. 2015). Prior to the September 2013 event, there were 5 events on record that were classified as comparable to the 2013 event by the Colorado Climate Center. However, all except one of these storms took place in the spring and summer months, as would be expected from the climatology of the rainfall events presented in earlier.

Out of the events listed in Table 1, the Colorado Climate Center noted that the event that occurred on 1st-12th September 1938 near Fort Collins, Colorado was the most similar in timing and magnitude to the September 2013 event. Observers recorded 203-254 mm (8-10 inches) of rainfall and the surrounding region experienced severe flooding. However, there is not much else known about this event because the amount of recorded atmospheric data available from this time period is limited. Comparing the September

2013 event to the 5 previous events in Table 1, this event had the highest total rainfall and caused the most damage, as is seen by the total cost of the event. This event also had a vast areal coverage, with heavy precipitation occurring from Denver all the way into southern Wyoming. Flooding took place as far to the east as Nebraska and caused a lot of damage to infrastructure along the Front Range of Colorado.

The amount of precipitation that fell during the September 2013 event required a large amount of moisture at a time of year when atmospheric moisture climatologically begins to decrease from higher summer values to lower winter values (Mahoney et al., 2015). This uncharacteric increase in moisture implies moisture was transported into the region. When moisture converges at the surface, it is transported to higher levels assuming there is sufficient atmospheric instability, which is usually greater over orography (Graham et al. 2012). The interaction of low level moisture with orography results in convection and the production of precipitation (Guerova et al. 2016). Adams et al. (2013) found that water vapor convergence which results in heavy precipitation generally occurs approximately an hour prior to the event. They also found that the stronger the convergence, the more intense the precipitation. Sapucci et al. (2016) found that after PW peaked, rainfall began and PW decreased.

Such characteristics are important to understand because they could influence future weather and climate trends. Kunkel et al. (2013) found an increasing trend in atmospheric PW quantities associated with extreme precipitation events and suggested this trend could lead to an increase in storm intensity. While Hoerling et al. (2014) noted that the September 2013 event was probably not connected to climate change, they did find that heavy precipitation events are becoming more frequent and Karl and Trenberth (2003)

found evidence that the number of heavy precipitation events is expected to increase with increasing global temperatures, such as we are experiencing now. The observed and projected increase in the number of heavy precipitation events, combined with the uncertainty of how PW contributes to characteristics of these events, motivated an investigation of PW characteristics surrounding the 2013 event so as to better understand the contributions of PW to an extreme precipitation event with the objective to someday apply these results to future research incorporating a wider variety of events.

As the aim of this research was to examine the characteristics of atmospheric PW during the 2013 Colorado Flood, data with a high spatial and temporal resolution was needed to resolve features within the event. GPS receivers are much more densely spaced with a total of 236 stations over North America than the radiosonde network, which has a total of 92 stations. The higher density of observations in the GPS network results in a higher spatial resolution with which to analyze storm features and water vapor transport. GPS data also has a much higher temporal resolution of anywhere from 30 minutes to two hours, as compared to the standard, twice-daily launching of radiosondes.

The primary goal of this research was to investigate the magnitude and characteristics of PW over the Front Range region associated with the September 2013 event. The goal of this study was to answer the following scientific questions.

(1) What were the characteristics of PW surrounding this event? This portion of research was focused on the examination of the temporal variability of PW, as well as a comparison with climatology, before, during, and after the event.

(2) Where did the moisture for the 2013 event originate? To answer this question, synoptic-scale dynamics and pre-existing conditions that led to large-scale, continuous moisture transport were evaluated.

2. Data and Methodology

2.1 Precipitable Water Datasets

Two datasets were used to analyze PW characteristics surrounding the 2013 event. The first of these was a two-hourly, long-term (1995-2015) PW dataset (Wang et al. 2007; Mears et al. 2015; Mears et al. 2016). The PW in this dataset is derived using 5-minute International Global Navigation Satellite System (GNSS) Service (IGS) Zenith Total Delay (ZTD) data. The analysis technique for the interpolation and conversion of ZTD to PW is summarized in Wang et al. (2007) and two key variables used in the conversion are water-vapor-weighted atmospheric temperature (Tm) and surface pressure (Ps). ZTD is represented as the sum of the Zenith Hydrostatic Delay (ZHD), which is a function of Ps, and the Zenith Wet Delay (ZWD), which is a function of PW and Tm. The 2-hourly PW data from Boulder became available starting in 2004.

The second PW dataset used in this study was the 30-minute SuomiNet dataset from the Constellation Observing System for Meteorology, Ionosphere, and Climate (COSMIC) group (Ware et al. 2000). The SuomiNet network currently consists of over 200 sites located around North America and the data are processed in near-real time from raw GPS data, the values of which do not differ greatly from post-processed GPS data. For this research, the standardized anomalies of the SuomiNet data were calculated by subtracting PW at each time step from the mean and dividing this by the standard deviation (Grumm and Hart 2001). The standardized anomaly data were gridded and

interpolated using a general kriging method to a grid box of 0.5°X0.5°. Kriging is defined as optimized interpolation that is weighted by spatial covariance values and based on regression against observed values of surrounding data points (Bohling 2005). This method was chosen because of its simplicity and superior performance when compared with the inverse distance weighting (IDW) method (Zimmerman et al. 1999; Yasrebi et al. 2009).

2.2 Formulation of a GPS PW Climatological Dataset

PW data for Boulder, Colorado were chosen to evaluate the PW variability of this region over the course of 10 years and compare this variability with that of 2013 to improve the understanding of how the September 2013 event differed from climatology. This region encompasses six SuomiNet stations and two IGS stations (Fig. 1b). To examine the anomalous nature of the flood, a dataset with a length of at least 10 years of observations was needed as a climatological standard for the analyzed region. While 10 years is not long enough for a standard climatology of 30 years as defined by the World Meteorological Organization (WMO), GPS PW data for Boulder has only been available since 2004. The PW time series of each GPS station was initially examined to determine which, if any, station had a long enough data record to serve as the climatological standard, and also to check for data outliers and data continuity. No stations were found to have more than seven years of data and datasets that contained discontinuities were discarded. A major issue that appeared during this analysis was that only one SuomiNet and one IGS station had data observations during the September 2013 event, and neither of them had a lengthy dataset. A decision was made to combine the data from different

227 stations in the region and make a 10-year dataset that included observations from the
228 flood.
229 The GPS PW data used to create the 10-year dataset were first quality-controlled by
230 using several methods defined in Wang et al. (2007). The first method used was the range
231 test in which the lower and upper limits of PW values were set as 0mm and 150mm,
232 respectively. The second quality-control method used involved using the mean and
233 standard deviation for each month to detect any outliers. This method required that at
234 least one-quarter of the data be present in order to have an adequate amount of
235 observations so that the statistical aspects could be deemed accurate. Individual PW
236 values within each month were analyzed and any values that were more than 4 standard
237 deviations away from the monthly mean were discarded (Wang et al. 2007). The quality
238 control removed 0.1% of the total data points for the station SA00 and less than 0.1% of
239 the total data points for the rest of the stations.
240 The next step in the creation of the 10-year dataset was to compare PW data among
241 the stations. PW is strongly dependent on elevation so any station that had an elevation
242 above 1,800 m was eliminated because these receivers were located too far above the
243 elevation of Boulder (1655 m). To remain consistent, the remaining stations were
244 compared to the station with the longest dataset and elevation closest to that of Boulder
245 (DSRC). Five stations were chosen for the merged 10-year PW dataset (Fig. 2) because
246 their averaged PW differences were not statistically significant from one another and the
247 elevation differences between all stations were less than 50 m. A more thorough analysis
248 of the complete dataset and its comparison with 2013 is described in Sect. 3. The
249 SuomiNet station, P041, also passed the statistical significance test, but did not have a

complete record of data for 2013 so could not be included in the 10-year dataset. Instead, the 2013 PW data from P041 was used to analyze small-scale variability leading up to, and during, the flood period because it has a higher temporal resolution (30 minutes) than NIST (two-hourly), which was chosen for the 10-year dataset.

2.3 Additional Datasets

The data used as a long-term PW climatology dataset were twice-daily radiosonde data from the Stapleton airport in Denver, Colorado extracted from the homogenized radiosonde dataset created by Dai et al. (2011). This PW dataset was created by integrating specific humidity from the surface to 100hPa, is available from 1979 to 2013, and was homogenized using an advanced statistical approach that is more thoroughly described in Dai et al. (2011).

The primary dataset used to evaluate moisture transport was the North American Regional Reanalysis (NARR) dataset, which is available from 1979 to the present (Mesinger et al. 2006). The domain for NARR is North America and the horizontal resolution is 32 km with 45 vertical layers. The NARR variables chosen for the evaluation of moisture transport surrounding the event were the 500 hPa geopotential height and the vertically integrated moisture flux.

3. Precipitable Water Characteristics

Gochis et al. (2015) noted that the atmosphere over Northern Colorado was abnormally moist from 9th-16th September. Radiosondes captured PW values above 30 mm, an abnormal value for a semi-arid climate. Gochis et al. (2015) also noted that the raindrop distribution during the event consisted of numerous small raindrops, which is more commonly observed in a tropical climate. To better understand how abnormal the

atmospheric moisture was during this event, the magnitude, distributions, and variability of PW over Boulder were evaluated and compared to climatology.

3.1 Temporal Variability of Precipitable Water

First, the temporal characteristics of September of 2013 were compared with the 10-year GPS PW dataset described in Sect. 2.2. Figure 2 shows the time series of the merged 10-year PW dataset discussed in Sect. 2. The strongest PW variation is seasonal with a mean seasonality of 18mm and the summer peaks are coincident with the annual occurrence of the wet season in Colorado. Also note that the belted appearance of this time series represents synoptic and diurnal PW variability, the latter of which has an average magnitude of 8 mm. The maximum value of PW for 2013 was 33.5 mm on September 12th. Note the extension of high PW values from the summer months into early September of 2013. This extension is not observed in any of the other years contained in this dataset and is an indication that the atmosphere was anomalously moist for the time of year in which the flood occurred.

Figure 3 zooms in on the extension of high PW values observed in September of 2013, giving a clearer view of the temporal variability of PW and precipitation surrounding the flood event. The high PW values up until 5th September represent moisture associated with the end of the North American Monsoon. These high values begin to decrease around 6th September before quickly rising on September 9th into the 10th, with values spiking to above 30 mm. PW decreases slightly to 26 mm until the 11th, when it once again increases to above 30 mm where it remains until the 13th. After this, PW decreases to values closer to the September climatological average of 15 mm.

PW peaks approximately one hour before rainfall begins, which is consistent with the findings of Adams et al. (2013) and Sapucci et al. (2016), both of which found that PW peaks between 32 and 64 minutes prior to the start of rainfall. Also consistent with their findings is the decrease of PW after it peaks. This is associated with the condensation of PW as it makes the transition into precipitation (Van Baelen et al. 2011). Another point to take note of is precipitation begins after PW rises between 2 and 3 standard deviations above the PW long term median, which was found in Foster et al. (2003).

An interesting point to take note of is that PW values stay relatively constant during the event despite the fact that continuous, and sometimes heavy, precipitation is occurring. For PW to remain at high values over multiple days, as was seen here, moisture needed to be continuously transported into the region (Gimeno et al. 2012). Had there not been a constant transport of moisture, PW would have decreased as atmospheric moisture condensed and formed precipitation. The examination of the moisture transport that fueled this event is presented in Sect. 4.

3.2 Precipitable Water Abnormality During the 2013 Flood

The consistently high values of PW during the time of heaviest precipitation in Fig. 3 led to an investigation to discern if the atmosphere over Boulder was fully saturated during the September 2013 event. To evaluate this, observed radiosonde PW data were compared with PW values that were calculated assuming a fully saturated atmosphere, i.e. 100% relative humidity from the surface up to 300 hPa. Note that a fully saturated atmosphere is an unrealistic assumption for a real atmosphere, but can be used for simplified comparison. Figure 4 shows the comparison between these two variables from 1st-28th September 2013. Starting on 10th September observed and fully saturated PW

318 values were within 5 mm of each other, indicating an atmosphere that was very near to
319 saturation during the course of the September 2013 event. Except for a period of time on
320 14th September when the atmosphere began to dry, observed PW stayed relatively close
321 in value to the fully saturated PW until 16th September.
322 Figure 5 compares monthly-averaged 2013 GPS data and radiosonde data to 40 and
323 10 years of monthly-averaged radiosonde and GPS data, respectively. 2013 PW monthly
324 averages were consistently lower than climatology until July while the Front Range was
325 still under drought conditions according to the National Climatic Data Center (NCDC)
326 North American Drought Monitor. The monthly average for September of 2013 was
327 around 20 mm, approximately 25% higher than the long-term climatological monthly
328 average for September. Also note that the monthly average for September of 2013 is
329 above the 95th and 99th percentiles, which were calculated from 40 years of monthly
330 averaged radiosonde data. McKee and Doesken (1997) evaluated extreme precipitation
331 events for Colorado from the late 1800's up until 1996 and found that, for these events,
332 PW never exceeded the 95th percentile. That the monthly averaged PW for September of
333 2013 exceeded the 99th percentile when compared to 40 years of data shows just how
334 anomalous the event was in terms of PW magnitude and timing.
335 Another tool used to evaluate how anomalous the 2013 Event was in terms of PW
336 was to examine the PW frequency distributions. Foster et al. (2006) examined the
337 monthly and annual frequency distributions of PW data for various stations and found
338 that there were three main types of distributions for PW data: lognormal, which is the
339 most common distribution around the world; reverse-lognormal, which represents an

atmosphere near saturation; and bimodal, which occurs in regions with strong seasonal variability such as monsoonal zones.

To analyze PW frequency for this event, monthly distributions were created for June through September of 2004-2013 (Fig. 6). The skewness of each distribution was then calculated and these values, along with visual analysis, were used to determine if each distribution was normal, lognormal, reverse-lognormal, or bimodal. Bulmer (1979) provided guidelines for interpreting the skewness of a distribution that were employed when evaluating the distributions in this study. A normal distribution has a skewness from -0.5 to 0.5, while a positive (negative) skewness with its absolute values within 0.5 to 1 represents a lognormal (reverse-lognormal) distribution (Bulmer 1979; Foster et al. 2006).

Upon analyzing the distributions in Fig. 6, June through September primarily have normal distributions with September being, on average, slightly more positively skewed than the other months with a value of 0.32, although the distribution is still considered normal according to the conditions for skewness defined in Bulmer (1979). However, the seasonal variation in PW is still evident as July and August distributions tend to have their highest frequencies over higher values of PW than either June or September. Also, despite most months having a normal distribution, there are four distributions which were labeled as lognormal because they have skewness values larger than 0.5: July 2005, September 2008, September 2010, and June 2013.

The distribution that shows the largest shift in distribution from the other years is that of September of 2013, which had a bimodal distribution. Figure 7 shows a more detailed comparison of September of 2013 PW data with 10 years of GPS PW data and 40 years

of radiosonde PW data. September of 2013 PW data were split up into two categories: "Flood", which represents 1st-15th September; and "Post-Flood", which represents 16th-30th September. Fig. 7 shows how different September of 2013 is from climatology and also how the atmosphere during the "Flood" differed from the "Post-Flood" atmosphere. The atmosphere during the "Flood" was highly saturated, with a peak frequency around 25 mm and PW values as high as 35 mm. The frequency distribution during this time was normal with a skewness value of 0.175. The "Post-Flood" atmosphere had a distinct lognormal distribution indicated by visual analysis and also by a skewness of 0.6838. The atmosphere at this time was considerably drier, with frequency peaking at 0.9 around 7 mm of PW.

4. Water Vapor Transport

The occurrence of heavy precipitation such as was observed during the September 2013 event requires sufficient moisture supply to fuel it. In Sect. 3, PW was shown to spike rapidly prior to the flood and remain at highly anomalous values for the duration of the event. In order to more completely understand the PW characteristics of this event, it was important to investigate where the moisture originated and what mechanisms were controlling the moisture transport that kept the atmosphere very near to saturation for seven consecutive days.

The moisture source and transport for the September 2013 event was briefly investigated in previous literature. Gochis et al. (2015) noted that the sources of moisture for the event were the Gulf of Mexico and the eastern tropical Pacific Ocean, both of which had 1-3 °C above normal sea surface temperature (SST) anomalies. They stated that the moisture from these regions was transported into the Front Range by a cutoff low

386 over the southwestern United States working in conjunction with an anticyclone over the
387 southeastern United States. Both of these features were kept in place for multiple days by
388 a blocking ridge located over the Canadian Rockies (Gochis et al. 2015). Trenberth et al.
389 (2015) stated that the source of moisture for the September 2013 event was only from the
390 eastern tropical Pacific Ocean, while Mahoney et al. (2015) claimed the moisture for the
391 event came primarily from the Gulf of Mexico.

392 Due to the slight variation of opinion on which body of water was the source of
393 moisture for the event, this study further investigates moisture source and transport by
394 examining NARR 500 hPa geopotential height and integrated water vapor flux in
395 conjunction with the standardized anomaly of gridded SuomiNet PW data. Five times
396 surrounding the event were chosen for analysis based on their proximity to rapid
397 fluctuations in PW (Fig. 3). The three variables listed above are plotted in Fig. 8 at each
398 of the five time steps.

399 Figure 8a-c shows the atmospheric conditions on 6th September at 9 UTC, prior to the
400 start of the event. There was a large ridge with 500 hPa geopotential heights above 596
401 gpm over the western half of the United States (US) (Fig. 8a) which contributed to higher
402 temperatures and dried the atmosphere over Boulder as seen in Figs. 3 and 8c. At that
403 point, there was no direct water vapor transport from either the Gulf of Mexico or the
404 eastern Pacific (Fig. 8b).

405 Moving on to 9th September at 18 UTC (Fig. 8d-f), a trough started to form over the
406 western United States and an anticyclone shifted over the southeastern US (Fig. 8d).
407 Together, these began transporting water vapor towards the northeast along the eastern
408 flank of the trough from the eastern Pacific (Fig. 8e). This transport contributed to a belt

409 of PW anomalies with magnitudes of 1.5 to 2.5 standard deviations over the southwestern
410 and western US (Fig. 8f). The PW anomaly over Boulder at that point was between 1-1.5
411 standard deviations and precipitation had not yet begun (Fig. 3). At this point, PW values
412 started to rise at a fairly quick rate (Fig. 3). This coincided with Adams et al. (2013) who
413 found that water vapor increases by low-level moisture convergence due to large scale or
414 other forcings. Water vapor appeared to travel to Colorado from the eastern Tropical
415 Pacific at that time (Fig 8e).

416 By 11th September at 6 UTC (Fig. 8g-i), the low pressure over the western US
417 deepened and formed into a cut-off low (Fig. 8g). The low stagnated over the western US
418 due to the influence of the blocking ridge under which it resided. The anticyclone over
419 the eastern US also strengthened. Working in conjunction, the strengthening of the low
420 and the high increased the southerly water vapor transport and there was a corridor of
421 flux convergence over New Mexico and the direction of the flux over Northern Colorado
422 was toward the Rocky Mountains (Fig. 8h). This resulted in a corridor of PW anomalies
423 that stretched from the Mexican border to southern Wyoming (Fig. 8i). The magnitude of
424 the PW anomaly over Boulder rose to between 2.5 to 3 standard deviations as the
425 moisture pooled against the Rocky Mountains due to easterly water vapor transport.
426 Light, orographically enhanced precipitation began and Boulder experienced rain rates
427 around 5mm h^{-1} (Fig. 3). Water vapor was being transported into Colorado from the
428 eastern Tropical Pacific and the Gulf of Mexico at this time (Fig 8h).

429 By 12th September at 6 UTC (Fig. 8j-l), the anticyclone began to break down but the
430 cutoff low deepened even further (Fig. 8j). Water vapor was still being transported into
431 the region from the Gulf of Mexico by the synoptic conditions with an easterly

component of the flux continuing to pool water vapor against the Rocky Mountains (Fig. 8k). However, the transport of moisture into Colorado appeared to have weakened substantially and the eastern Tropical Pacific was no longer a source of moisture. There was still a corridor of PW anomalies coinciding with the regions of strong water vapor flux and the magnitude of the anomaly over Boulder was still between 2.5 to 3 standard deviations (Fig. 8l). Precipitation intensified over the past 24 hours and Boulder experienced up to 35mm h^{-1} of rainfall (Fig. 3). While a majority of the rainfall was orographically-enhanced, the occasional intense periods of rainfall were a result of mesoscale circulations, as was noted by Gochis et al. (2015).

By 14th September at 21 UTC (Fig. 8m-o), the blocking ridge broke down, which allowed synoptic conditions to shift eastward, and the cutoff low once again became a trough (Fig. 8m). This resulted in the water vapor flux also shifting eastward (Fig. 8n). The PW anomaly over Boulder decreased to between 1 to 2 standard deviations (Fig. 8o). Rainfall for the event ended at this point, excluding a peak that occurred during the afternoon of 15th September (Fig. 3).

Upon comparing NARR integrated moisture flux with 500 hPa geopotential height and observed standardized PW anomalies, it was found that the strength and location of moisture transport varied over the course of the event. Prior to the event, on 9th September, moisture from the eastern tropical Pacific appears to have been transported up to Colorado by a stagnating cutoff low over the southwestern US. Starting on 10th September, the cutoff low and subtropical anticyclone promoted southerly flow into Colorado from the eastern tropical Pacific and the Gulf of Mexico. As of the 12th September, the eastern tropical Pacific no longer provided moisture for the event and the

Gulf of Mexico was the sole source of moisture. By the 14th September, the transport of moisture into Colorado had significantly weakened due to the eastward shift of the synoptic pattern. The moisture transport was dependent on the strength and location of the dominant synoptic features, and based on the analysis shown in Fig. 8 the moisture has been transported into Colorado from both the Eastern Tropical Pacific and the Gulf of Mexico. These results are most consistent with the findings of Gochis et al. (2015), but do not discount the results found in Trenberth et al. (2015) and Mahoney et al. (2015).

5. Conclusions

The aim of this research was to analyze PW characteristics surrounding the September 2013 event and compare them to climatology. Precipitation began approximately an hour after PW rose to between 2 and 3 standard deviations above the PW long-term median. This result was consistent with past literature that rxamined the relationship between PW and precipitation. Monthly averaged PW values in the GPS dataset for September of 2013 was above the 99th percentile when compared to the climatological data as well as around 25% higher than the monthly-averaged climatological mean value for September. That the monthly average for September of 2013 was so far above the climatology for 10 and 40 years of data indicates how anomalous the atmospheric moisture content was during the event. The frequency distribution of PW for September of 2013 was bimodal, which was much different than the typical normal distribution observed in September of other years. Upon further analysis, it was noted that the highly saturated portion of the bimodal distribution was solely the result of the September 2013 event, which had a nearly saturated atmosphere. The second half of September had a lognormal distribution, representing a much drier

atmosphere for the rest of the month. The moisture for the event originated from the eastern tropical Pacific at the beginning of the event 9th September, came from this source and the Gulf of Mexico during the heaviest precipitation (10th – 12th September), and then from only the Gulf of Mexico towards the end (12th-14th September).

Code Availability

Code is available from the lead author upon request.

Data Availability

Two-hourly GPS PW data is available upon request from the first and second authors. 30 minute SuomiNet GPS PW data is available for download in ASCII and NetCDF format from the COSMIC group website (suominet.ucar.edu). The twice daily, homogenized radiosonde data is available upon request from the second author. NARR data is available for download on the National Oceanic and Atmospheric Administration (NOAA) website (nomads.ncdc.noaa.gov/data/narr). The 1-hourly rain gauge data is available upon request from the National Center for Atmospheric Research (NCAR) Research Applications Laboratory (RAL).

Appendix A – List of Figures

Fig. A1. (a) Map of accumulated precipitation over Colorado from 8-15 September 2013 (image courtesy of the Colorado Climate Center) with the area depicted in (b) outlined in the black box; and (b) the locations of the primary GPS (blue circles), rain gauge (green circle), and radiosonde (red circle) observations used in this study. NISU and NIST are the only IGS GPS stations plotted on this map. All of the other GPS stations are from the SuomiNet network.

Fig. A2. A time series of the GPS PW data for Boulder, Colorado from 2004-2013 with each station denoted by a different color, the monthly means denoted by the solid, black line, and +/- 1 standard deviation denoted by the horizontal, black, dashed lines. September of each year is represented by the vertical black lines.

Fig. A3. A time series of 30-minute (station P041) and 2-hourly (station NIST) GPS PW compared with precipitation (rain gauge UDFCD4840) from 1-28 September 2013. The inserted graph compares the same variables from 9-14 September 2013 with the addition of lines indicating 1, 2, and 3 standard deviations above the PW long-term median.

Fig. A4. A time series comparison of observed radiosonde PW (black line) and saturated PW (green line) for 1-28 September 2013 over Denver, Colorado.

Fig. A5. Monthly-averaged GPS PW (solid black line) and Radiosonde data (dashed black line) for 2013 with the 10-year merged GPS PW dataset (solid red line) and the 40-year averaged Radiosonde PW dataset (solid blue line). Additionally, there are the 95th (dashed red line) and 99th (dotted red line) percentiles for 10 years of GPS data and the 95th (dashed blue line) and 99th (dotted blue line) percentiles for 40 years of Radiosonde data.

Fig. A6. Statistical frequency distributions of GPS PW for June- September of 2004-2013 with the 95th percentile for 10 years of each month of data denoted by the left-most dashed line and the 99th percentile for 10 years of each month of data denoted by the right-most dashed line.

Fig. A7. Statistical frequency distributions for the month of September with 2013 GPS PW data over Boulder (black line), 40 years of climatologically-averaged radiosonde PW data over Denver (dark grey line), and 10 years of climatologically-averaged GPS PW

data over Boulder (light grey line). September of 2013 GPS PW data was split into two halves: 1-15 September 2013 (Flood; green line), and 16-30 September 2013 (Post-Flood; blue line).

Fig. A8. A comparison of NARR 3-hourly averaged 500hPa geopotential height (left column), NARR 3-hourly averaged integrated water vapor flux (center column), and SuomiNet gridded standardized PW anomalies. Each row represents a different time surrounding the 2013 Event.

Appendix B – List of Tables

Table B1. A comparison of the September 2013 event to previous flood inducing, heavy precipitation events in Northern Colorado history. All monetary values were calibrated to 2013 values.

Table B2. The geographic and topographic information of the primary GPS, rain gauge, and radiosonde stations used in this study.

Author Contribution

The first author was the primary researcher with constant assistance and guidance from the second author. The third author was the PI on the grant and a contributing editor. The fourth author served as an editor.

Competing Interests

There are no competing interests from any of the authors.

Disclaimer

There is no disclaimer regarding the research completed in this paper.

Acknowledgements

This research was supported by the National Aeronautics and Space Administration (NASA) RSS Subcontract #6003 under the Prime Contract NNX11AO25A. The authors would like to thank David K. Adams and the two anonymous reviewers for their valuable input during the review process

Works Cited

Adams, D. K., S. I. Gutman, K. L. Holub, and D. S. Pereira, 2013: GNSS Observations of Deep Convective Time scales in the Amazon. Geophys. Res. Lett., 40. doi:10.1002/grl.50573.

Bohling, G., 2005: Introduction to geostatistics and variogram analysis C&PE 940. Kansas Geol. Surv.

Bulmer, M. G., 1979. Principles of Statistics. Cambridge, MA: M.I.T. Press.

Colorado Climate Center, Colorado Flood 2013 Storm Page, published online October 2013.

Dai, A., J. Wang, P.W. Thorne, D.E. Parker, L. Haimberger, and X.L. Wang, 2011: A new approach to homogenize daily radiosonde humidity data. J. Climate, 24, 965-991.

Foster J., Bevis M., Chen Y.-L., Businger S., and Zhang Y., 2003: The Ka`u Storm (Nov. 2000): Imaging precipitable water using GPS. J. Geophys. Res. 108, 4585.

Foster, J., M. Bevis, and W. Raymond, 2006: Precipitable water and the lognormal distribution. J. Geophys. Res.,111.D15102, doi:10.1029/2005JD006731.

Gimeno, L., A. Stohl, R. M. Trigo, F. Dominguez, K. Yoshimura, L. Yu, A. Drumond, A. M. Durán-Quesada, and R. Nieto (2012), Oceanic and terrestrial sources of

569 continental precipitation, Rev. Geophys., 50, RG4003,
570 doi:10.1029/2012RG000389.
571 Gochis, D., and Coauthors, 2015. The Great Colorado Flood of September 2013. The
572 Bulletin of the American Meteorological Society.
573 Graham, E., E. N. Koffi, and C. Matzler, 2012: An observational study of air and water
574 vapour convergence over the western Alps during summer and the development
575 of isolated thunderstorms. Meteorol. Z., 21, 1-13. doi:10.1127/0941-
576 2948/2012/0347.
577 Guerova, G., J. Jones, J. Douša, G. Dick, S. de Haan, E. Pottiaux, O. Bock, R. Pacione,
578 G. Elgered, H. Vedel, and M. Bender, 2016: Review of the state of the art and
579 future prospects of the ground-based GNSS meteorology in Europe, Atmos.
580 Meas. Tech., 9, 5385-5406, https://doi.org/10.5194/amt-9-5385-2016.
581 Hoerling, M., and Coauthors, 2014: Northeast Colorado extreme rains interpreted in a
582 climate change context [in "Explaining Extremes of 2013 from a Climate
583 Perspective"]. Bull. Amer. Meteor. Soc., 95 (9), S15–S18.
584 Karl, T. R., and K. E. Trenberth, 2003: Modern global climate change. Science, 302,
585 1719–1723.
586 Kunkel, K. E., and Coauthors, 2013: Monitoring and understanding trends in extreme
587 storms: State of knowledge. Bull. Amer. Meteor. Soc., 94, 499–514.
588 Maddox, R. A., Caracena, F., Hoxit, L. R., Chappell, C. F., 1977: Meteorological Aspects
589 of the Big Thompson Flash Flood of 31 July 1976. NOAA Technical Report.

590 Mahoney, K., Ralph, F. M., Wolter, K., Doesken, N., Dettinger, M., Gottas, D., Coleman,
591 T., White, A., 2015: Climatology of Extreme Daily Precipitation in Colorado and
592 Its Diverse Spatial and Seasonal Variability. Journal of Hydrometeorology.
593 McKee, T. B., and N. J. Doesken, 1997: Final report: Colorado extreme precipitation data
594 study. Climatology Rep. 97-1, Department of Atmospheric Science, Colorado
595 State University, 107 pp. Available from Colorado Climate Center, Department of
596 Atmospheric Science, Colorado State University, Fort Collins, CO 80523.
597 Mears, C, Ho, S., Peng, L., Wang, J., and Huelsing, H., 2015: Total column PW, in State
598 of the Climate in 2014. Bull. Amer. Meteorol. Soc., 96, S22-23.
599 Mears, C, Ho, S., Wang, J., Huelsing, H., and Peng, L., 2016: Total Column PW. Bull.
600 Amer. Meteorol. Soc., In Press.
601 Petersen, W.A., 1999: Mesoscale and Radar Observations of the Fort Collins Flash Flood
602 of 28 July 1997. Bulletin of the American Meteorological Society. Vol. 80, No. 2,
603 February 1999.
604 Sapucci, L. F., Machado, L. A. T., Menezes de Souza, E., and Campos, T. B.: GPS-PWV
605 jumps before intense rain events, Atmos. Meas. Tech. Discuss.,
606 https://doi.org/10.5194/amt-2016-378, 2016.
607 Van Baelen, J., M. Reverdy, F. Tridon, L. Labbouz, G. Dick, M. Bender, and M. Hagen,
608 2011: On the relationship between water vapour and evolution and the life cycle
609 of precipitation systems. Q. J. Roy. Meteor. Soc., 137, 204-223,
610 doi:10.1002/qj.785.

Wang, J., Zhang, L., Dai, A., Van Hove, T., and Van Baelen, J., 2007: A near-global, 2-hourly dataset of atmospheric precipitable water from ground-based GPS measurements. J. Geophys. Res., 112, D11107, doi:10.1029/2006JD007529

Ware, R. H., D. W. Fuller, S. A. Stein, D. N. Anderson, S. K. Avery, R. D. Clark, K. K. Droegemeier, J. P. Kuettner, J. B. Minster, and S. Sorooshian, 2000: SuomiNet: A Real-Time National Network for Atmospheric Research and Education. Bulletin of the American Meteorological Society, 81, 4, 677-694.

Yasrebi J, Saffari M, Fathi H, Karimian N, Moazallahi M, et al., 2009. Evaluation and comparison of ordinary kriging and inverse distance weighting methods for prediction of spatial variability of some soil chemical parameters. Research Journal of Biological Sciences 4: 93–102.

Zimmerman, D., Pavlik, C., Ruggles, A. and Armstrong, M. P., 1999. An experimental comparison of ordinary and universal Kriging and inverse distance weighting. Mathematical Geology, 31 (4).

Date	Location Most Affected	Total Rainfall (inches)	Deaths	Cost
September 1-12, 1938	Fort Collins	8-10	N/A	N/A
May 4-9, 1969	West of Denver	6-9	0	$136.5 million
July 31-August 1, 1976	Estes Park	12-14	144	$348.5 million
July 27-August 4, 1997	Fort Collins	14.5	5	$290 million
April 29-30, 1999	Northern Colorado	8-10	0	$140 million
September 9-16, 2013	Boulder	16	8	$2 billion

633

634 **Table 1.** A comparison of the September 2013 Event to previous flood inducing, heavy
635 precipitation events in Northern Colorado history. All monetary values were calibrated to
636 2013 values.

637

638

639

640

641

642

643

644

Station Name	Latitude (°N)	Longitude (°W)	Altitude (m)	Type of Station
72469	39.77	-104.87	1625	Radiosonde
DSRC	39.991431	-105.26103	1668.87	GPS
NISU/NIST	39.995	-105.2626	1648.488	GPS
P041	39.949492	-105.19427	1743.19	GPS
SA00	40.03516	-105.24327	1623.23	GPS
SA67	40.037568	-105.24086	1622.66	GPS
UDFCD_4840	39.9724	-105.2229	1645.92	Rain Gauge

645

646 **Table 2.** The geographic and topographic information of the primary GPS, rain gauge,

647 and radiosonde stations used in this study.

648

649

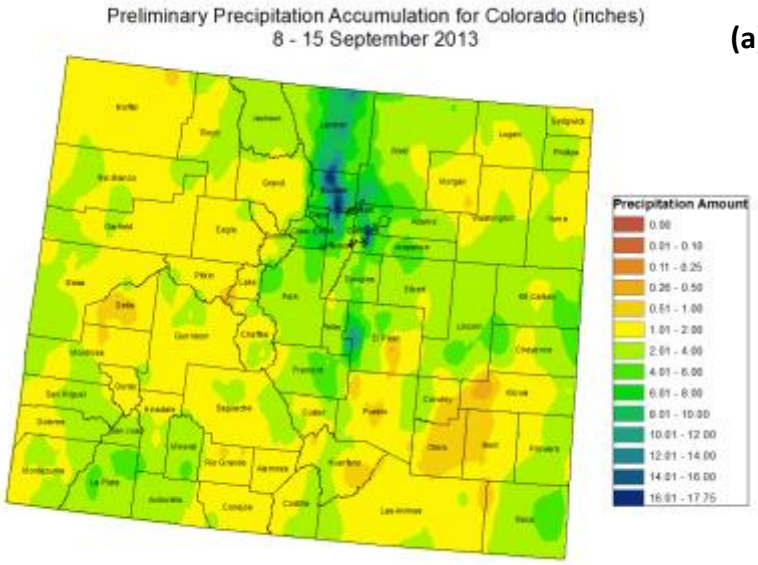

650

651
652 **Figure 1.** (a) Map of accumulated precipitation over Colorado from 8-15 September
653 2013 (image courtesy of the Colorado Climate Center); and (b) the locations of the
654 primary GPS (blue circles), rain gauge (green circle), and radiosonde (red circle)
655 observations used in this study. NISU and NIST are the only IGS GPS stations plotted on
656 this map. All of the other GPS stations are from the SuomiNet network.

657
658

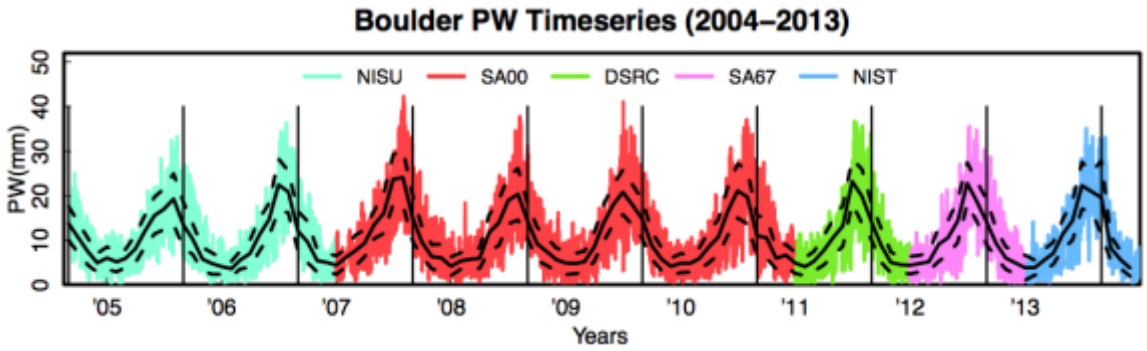

Figure 2. A time series of the GPS PW data for Boulder, Colorado from 2004-2013 with each station denoted by a different color, the monthly means denoted by the solid, black line, and +/- 1 standard deviation denoted by the horizontal, black, dashed lines. September of each year is represented by the vertical black lines.

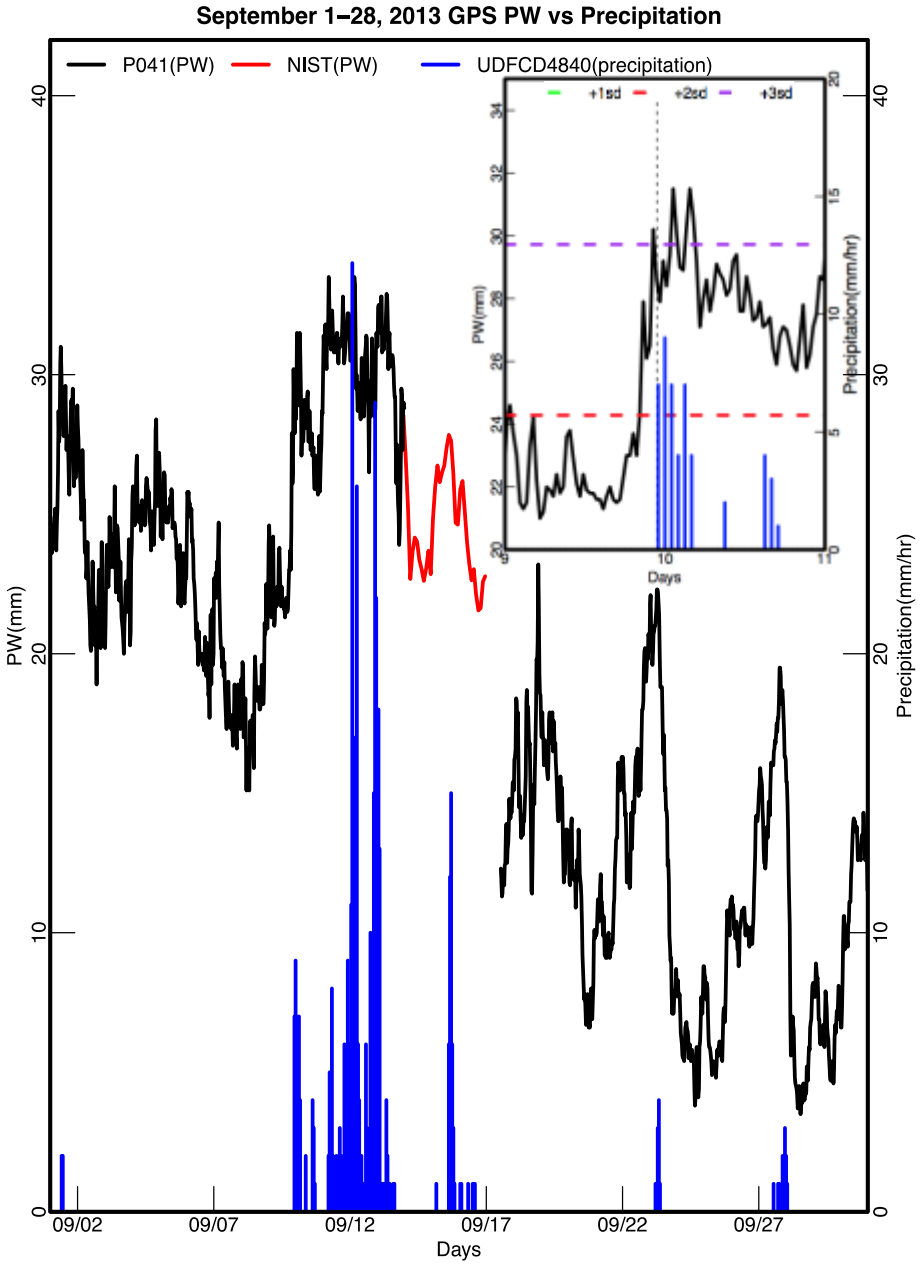

669
670 **Figure 3.** A time series of 30-minute (station P041) and 2-hourly (station NIST) GPS PW
671 compared with precipitation (rain gauge UDFCD4840) from 1 – 28 September 2013. The
672 inserted graph compares the same variables from 9 – 14 September 2013 with the
673 addition of lines indicating 1, 2, and 3 standard deviations above the PW long-term
674 median.

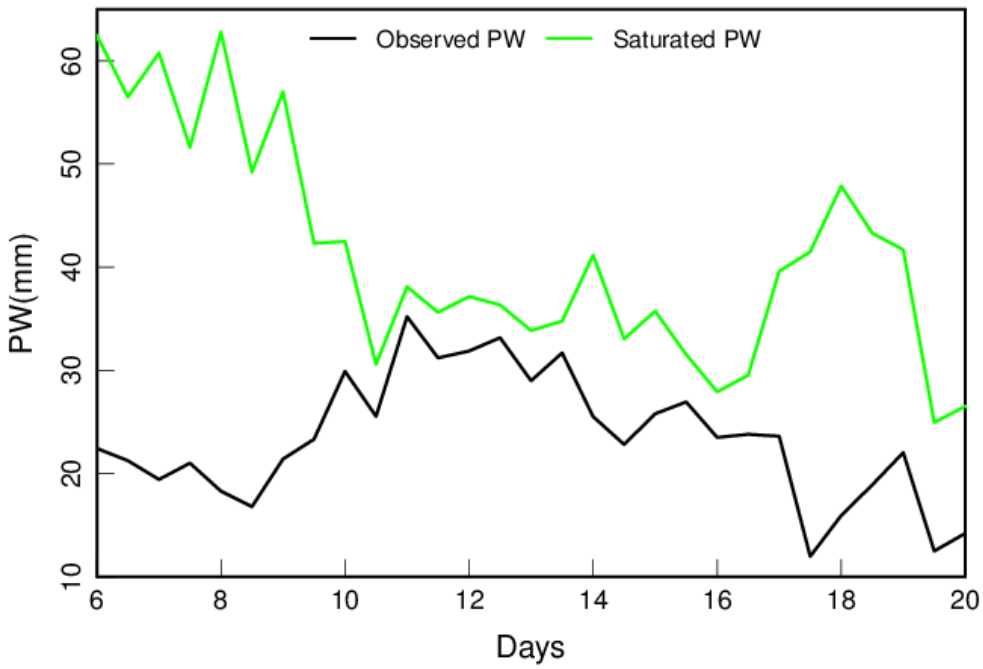

675
676 **Figure 4.** A time series comparison of observed radiosonde PW (black line) and saturated
677 PW (green line) for 6-20 September 2013 over Denver, Colorado.
678
679
680

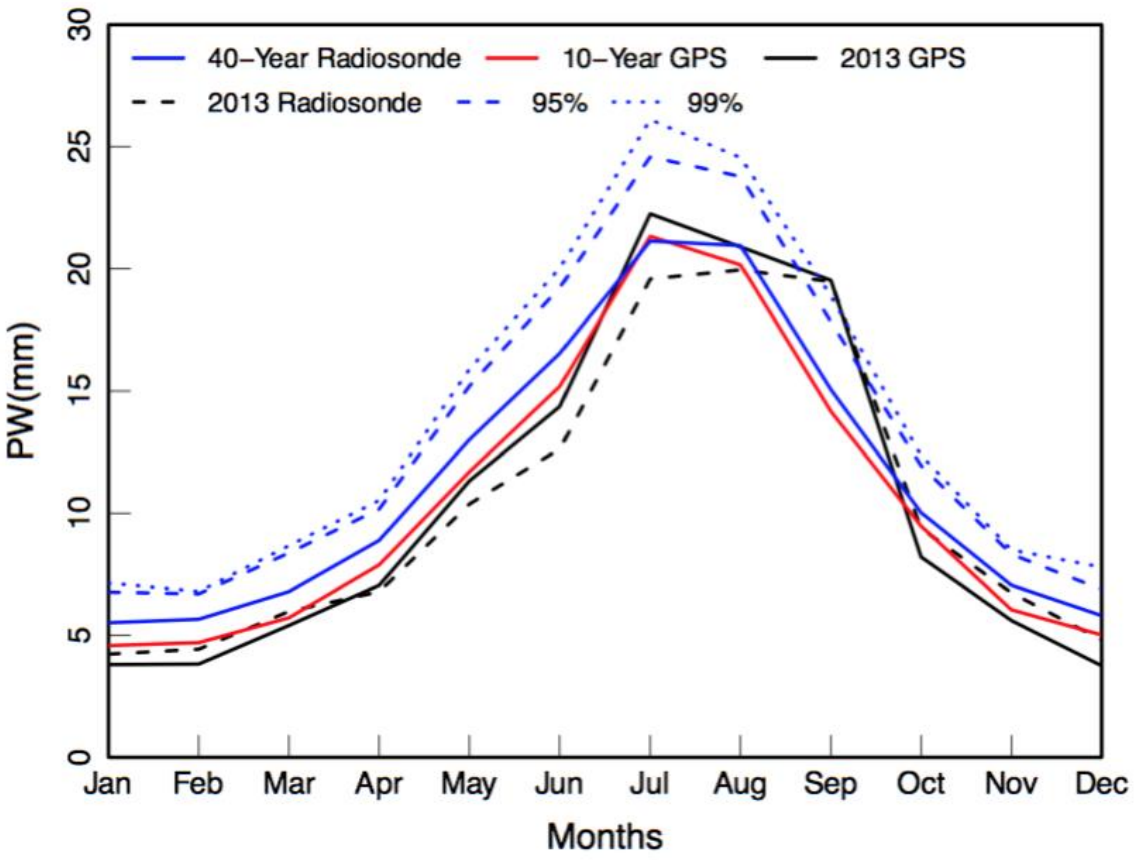

Figure 5. Monthly-averaged GPS PW (solid black line) and Radiosonde data (dashed black line) for 2013 with the 10-year merged GPS PW dataset (solid red line) and the 40-year averaged Radiosonde PW dataset (solid blue line). Additionally, there are the 95th (dashed red line) and 99th (dotted red line) percentiles for 10 years of GPS data and the 95th (dashed blue line) and 99th (dotted blue line) percentiles for 40 years of Radiosonde data.

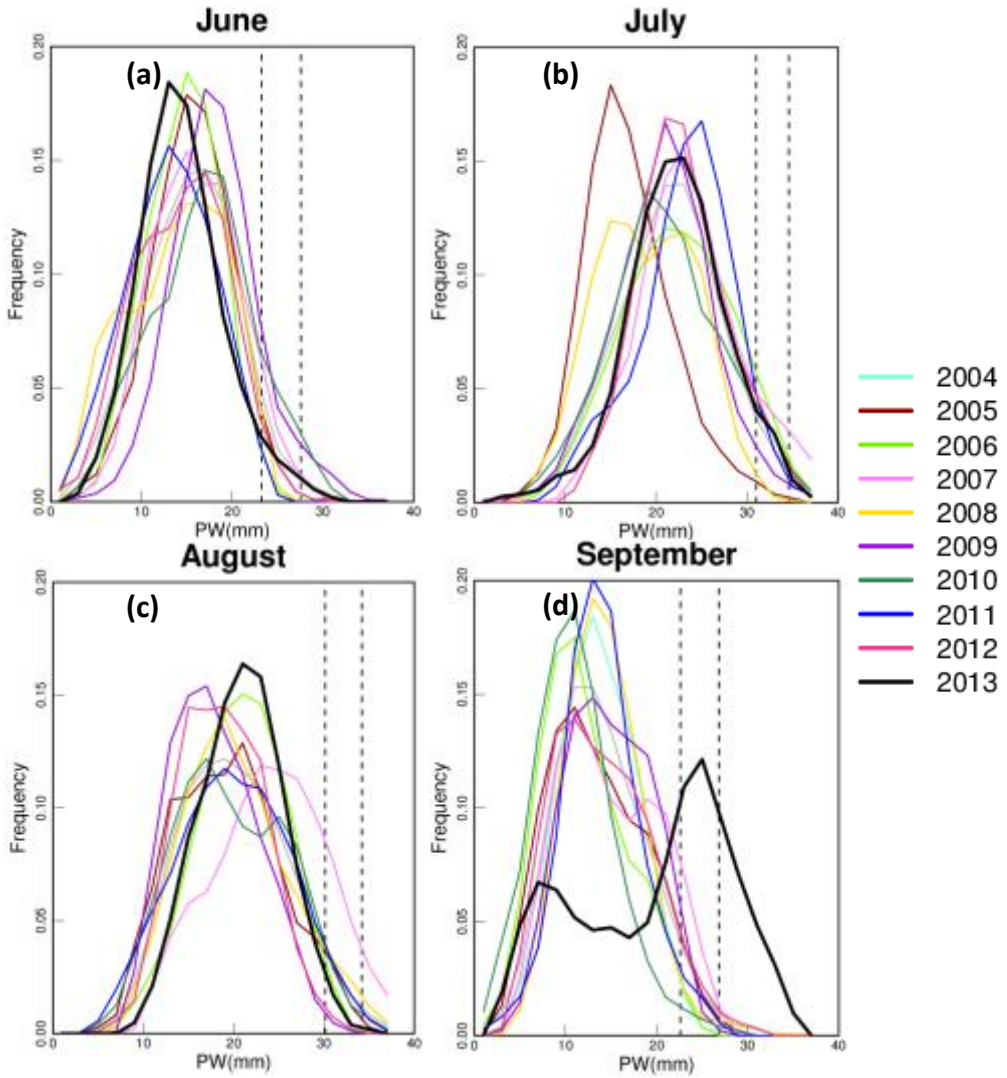

Figure 6. Statistical frequency distributions of GPS PW for June- September of 2004-2013 with the 95th percentile for 10 years of each month of data denoted by the left-most dashed line and the 99th percentile for 10 years of each month of data denoted by the right-most dashed line.

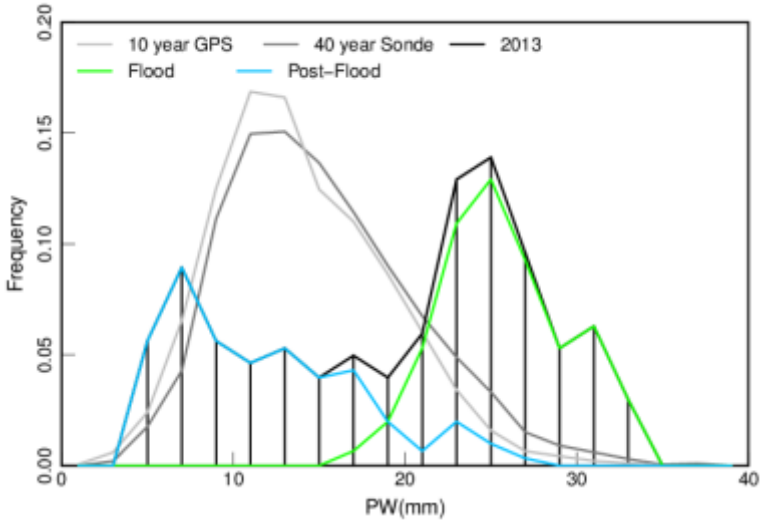

Figure 7. Statistical frequency distributions for the month of September with 2013 GPS PW data over Boulder (black line), 40 years of climatologically-averaged radiosonde PW data over Denver (dark grey line), and 10 years of climatologically-averaged GPS PW data over Boulder (light grey line). September of 2013 GPS PW data was split into two halves: 1-15 September 2013 (Flood; green line), and 16-30 September 2013 (Post-Flood; blue line).

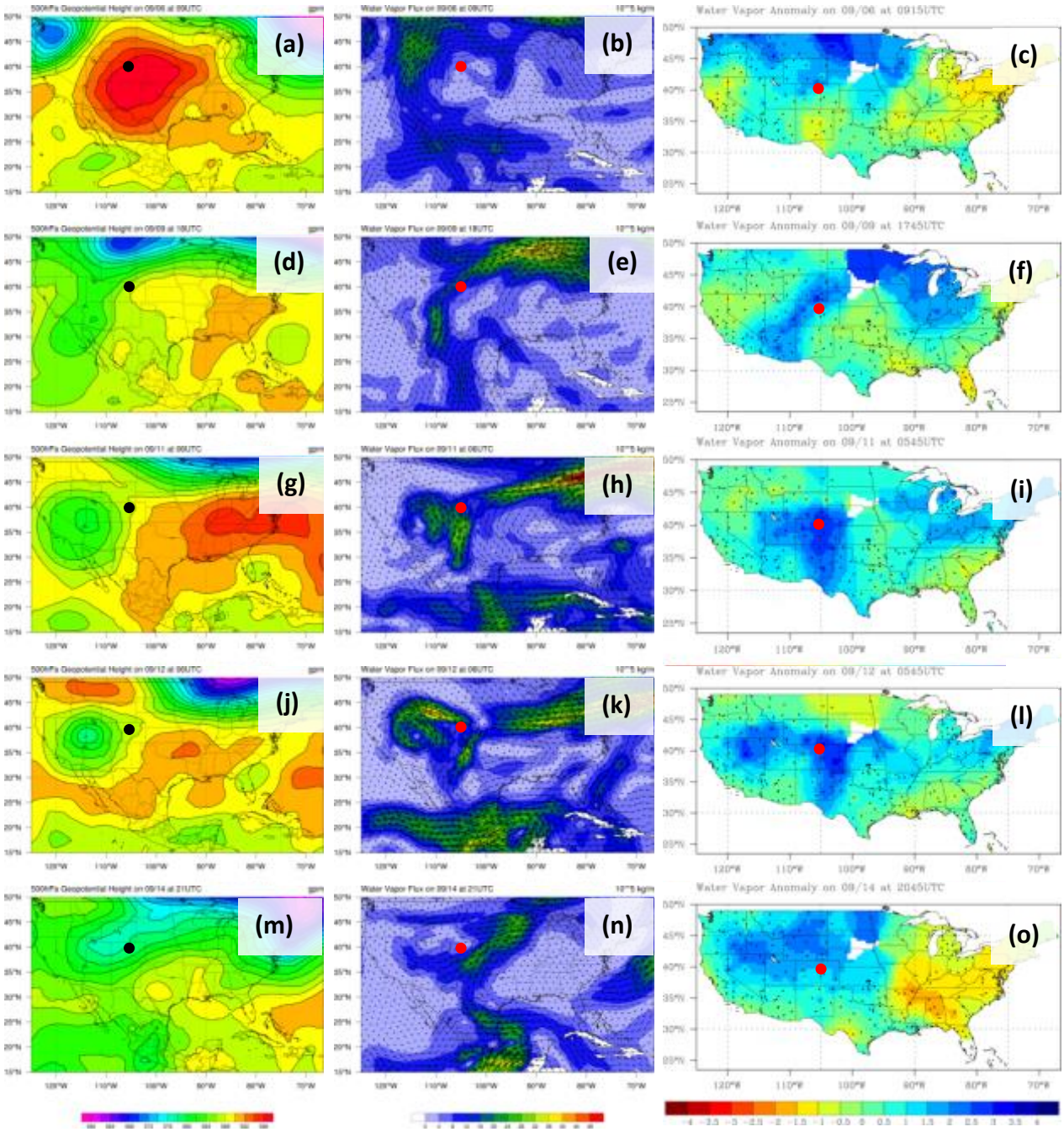

Figure 8. A comparison of NARR 3-hourly averaged 500 hPa geopotential height (left column), NARR 3-hourly averaged integrated water vapor flux (center column), and SuomiNet gridded standardized PW anomalies. Each row represents a different time surrounding the 2013 Event.